U.S. DEPARTMENT OF ENERGY
Office of ENERGY EFFICIENCY & RENEWABLE ENERGY

X-CEL:
eXtreme fast charge Cell Evaluation of Lithium-ion batteries

Jan 2019

Quarterly Report Period: Quarter 4 - 2018

Table of Contents

Project Overview

Venkat Srinivasan (Argonne National Laboratory), Samuel Gillard (Department of Energy)

DOE-EERE has identified fast charge as a critical challenge in ensuring mass adoption of electric vehicles with a goal of 15-min recharge time. Present day high energy cells with graphite anodes and transition metal cathodes in a liquid electrolyte are unable to achieve this without negatively effecting battery performance. There are numerous challenges that limit such extreme fast charging at the cell level, including Li plating, rapid temperature rise, and possible particle cracking. Of these, Li plating is thought to be the primary culprit. This project aims to gain an understanding of the main limitations during fast charge using a combined approach involving cell builds, testing under various conditions, characterization, and continuum scale mathematical modeling. Expertise from three National Labs are utilized to make progress in the project.

Cells are built at the Cell Analysis, Modeling, and Prototyping (CAMP) facility at Argonne National Lab (ANL) using various carbons, different cell designs, in both half-cell and full cell configuration and with reference electrodes. Cells are tested at both Idaho National Lab (INL) and ANL under various operating conditions (c-rate, temperature) and under different charging protocols with the aim of identifying the onset of plating, to quantify the extent of the problem, and to determine parameters and test data for mathematical models. Tested cells are opened and various advanced characterizing performed at ANL to determine the extent of plating and to determine if other failure models, such as particle cracking, also play a role.

A critical part of the project is the use of continuum scale mathematical models to understand the limitations at high charge rates and therefore suggest possible solutions that can be pursued. Both macro-scale approaches and microstructure-based simulations are pursued and serve to complement each other. Macromodeling at National Renewable Energy Lab (NREL) is used to test cell designs, accompanied by microstructure models to provide deeper insights into the phenomenon in the battery. This is complemented with development of models incorporating of new physics, such as phase change and SEI growth, at ANL.

Finally, two exploratory projects aim to study ways to detect Li *in situ* during operation. NREL will pursue the use of microcalorimetry to detect heat signatures during plating. INL will work with Princeton University to examine the use of acoustic methods to determine if plating leads to a signature in the acoustic signal.

In this quarter, data on cells with different loading is helping the team determine the extent to which fast charging can be achieved on high-loading cells. Using continuum-scale modeling it is becoming clear that the Li insertion reaction is non-uniform with higher current near the separator region. This reaction distribution pushes the anode towards the plating potential as the loading is increased. All evidence points to the need to ensure that the anode is utilized in a uniform fashion and minimize the non-uniformity. However, research in this quarter also shows that determining the exact point when Li plating occurs, both from experiments and from model predictions, is hard and capacity fade is an insufficient indicator of plating. Efforts are now underway to develop methods to enhance the detection capability for Li plating to accelerate the ability to test hypothesis for what limits the battery under these extreme charging conditions.

ANL: CAMP Facility Electrode and Cell Development for Fast Charge

Alison Dunlop, Andrew Jansen (PI), Bryant Polzin, and Steve Trask (Argonne National Laboratory)

Background

In this first year's effort, the Cell Analysis, Modeling, and Prototyping (CAMP) Facility's objective is to develop experimental electrodes that will be used to identify causes of lithium plating at fast charges in single-layer pouch cells. Earlier work at Argonne by Gallagher et al. [1] had studied the influence of capacity loading on material utilization at various discharge rates. This work also touched on the effect of charge rate on capacity retention and lithium plating, which is summarized in Figure 1. These single-layer pouch cells were originally charged for 285 cycles at a C/3 rate, after which the charge rate was increased to C/1 (followed by trickle charging to 4.2 volt [V]) up to 549 cycles, and for the surviving cells, the charge rate was further increased to 1.5C. The discharge rate was held at C/3 rate in all cases to remove that rate as a variable. As can be seen in Figure 1, it is clear that the electrodes with loadings higher than ~3 mAh/cm² could not sustain a charge rate higher than C/1.

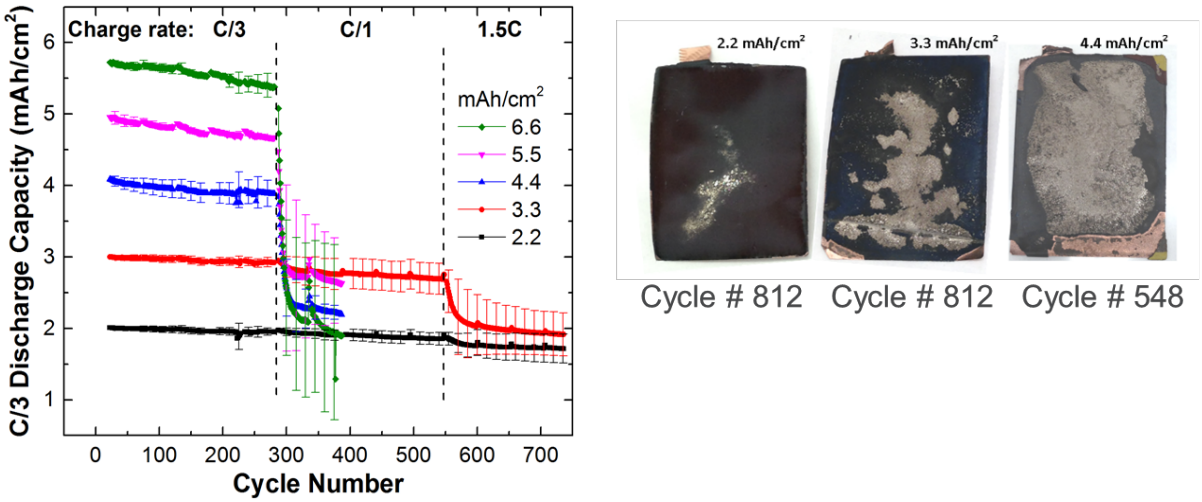

Figure 1. Discharge capacity as a function of electrode loading (mAh/cm²) and charge rate (left) and photos of lithium deposits on representative graphite electrodes (right). These results were obtained with capacity-matched cells using graphite negative electrodes and $LiNi_{0.6}Mn_{0.2}Co_{0.2}O_2$ (NMC622) positive electrodes.

Evidence of lithium plating was sought for these cells by disassembling representative cells in a dry room after a 24-h voltage hold at 3.75V and then washing with dimethyl carbonate. As expected, cells with the largest capacity fade exhibited the most lithium deposits as can be seen in Figure 1. Surprisingly, fully discharging one of the 4.4 mAh/cm² cells at a low rate before disassembly did not remove the lithium deposits from the negative electrode surface, which suggests that the lithium deposits becomes electrically isolated from the graphite electrode.

The goal of the work now is to determine the influence of graphite selection on fast charge capability, at an even faster rate of 6C. Initial expectations are that the physical properties of the graphite particles in the negative electrode will affect the onset of lithium dendrites. These properties include the surface area, particle size, size distribution, surface coatings/modifications, and source of graphite, i.e., natural graphite versus artificial graphite. The CAMP Facility has a range of graphite powders suitable for this study that can provide

a basis of comparison for these properties. At least four different graphite powders will be made into negative electrodes and evaluated for fast charge performance against a standard NMC532 positive electrode. This screening test will be performed in coin cells. The best performing graphite material will then be used in single-sided single-layer pouch cell builds and delivered to battery testing labs in this program for complete electrochemical characterization under fast charge conditions.

A second single-sided single-layer pouch cell build will be performed based on the preliminary results of the coin-cell graphite screening results and the first pouch cell build. This second cell build will either use a different graphite or a higher electrode mass loading (thicker). These pouch cells will also be delivered to the battery test labs for evaluation and analysis.

Results

Prescreening of Available Graphite Powders

Table 1 lists the available properties for the graphite powders selected in the prescreening tests initiated at the start of this fiscal year. Since several of these powders were already incorporated into the CAMP Facility's Electrode Library, it was decided to evaluate these materials using the Library's anode capacity loading of 2 mAh/cm² against capacity-matched NMC532 positive electrodes also in the Library. The n:p ratios were ~1.1 to 1.2. Graphite materials not in the Electrode Library were designed and developed at the same capacity loading (and added to the Library).

Table-1: Graphite powders selected to elucidate causes of lithium plating during fast charges.

Trade Name	Company	Type	Particle shape or morphology	Tap Density, [g/mL]	Surface Area, [m²/g]	Particle Size D10, [µm]	Particle Size D50, [µm]	Particle Size D90, [µm]
SLC1506T*	Superior Graphite	coated, natural graphite	spherical graphite powder	1.03	1.936	5.37	8.06	13.15
SLC1520P	Superior Graphite	coated, natural graphite	spherical graphite powder	1.19	0.89	11.03	16.94	26.76
MagE3	Hitachi	artificial graphite, combines hard graphite additive		0.90	3.9	-	22.4	-
MCMB	Gelon	Artificial, Mesocarbon Microbeads standard type-G15	MesoCarbon MicroBeads	1.324	2.022		17.649	
CPG-A12	Phillips 66	natural graphite core coated with surface treatment	potato	-	2 to 4	-	9 to 12	-

BTR-BFC-10	BTR	Artificial Graphite High Energy Fast Charge [Targray-SPGPT805]	TBD	0.770	2.487	6.539	11.196	18.891

Coin cells were assembled with 14 mm diameter cathodes and 15 mm diameter anodes using Celgard 2320 separator (20 µm, PP/PE/PP) and Tomiyama 1.2 M $LiPF_6$ in EC:EMC (3:7 wt%) "Gen2" electrolyte. Four duplicate coin-cells were made for each graphite. The coin cells were then cycled in the 3.0 to 4.1V window with 3 formation cycles at C/10 (w/ C/20 trickle charge), followed by 250 cycles of fast charging at 6C with trickle charge down to C/5 until a maximum charge time of 10 minutes was reached, with C/2 discharges. 2 minute open circuit rests were used between charge and discharge steps. This profile was repeated until <80% of the capacity measured at the 10^{th} cycle remained.

At this relatively low loading, all of the graphite materials in Table 1 were able to cycle under a 6C charge rate for 750 cycles, at which point they were removed from testing and given to the Post-Test Facility for tear down and inspection. A comparative summary of their capacity over cycling is best illustrated in Figure 2, which is the average of the cells (with standard deviations) for each graphite. This data was also analyzed in terms of capacity retention, and is summarized in Table 2. Cycle 10 was used as the common cycle in normalizing this data, which is a point where the majority of cells were considered to be stabilized. Surprisingly, nearly all cells have reached 750 cycles with 80% capacity retention. A few conclusions can be postulated here based on this data, namely: 1) these selected graphites are statistically similar at this relatively low capacity loading (2 mAh/cm²); 2) the difference between natural graphite and synthetic graphite is not significant; and 3) SLC1506T graphite and MCMB graphite appear to have higher capacity utilization compared to the other graphite materials. Although it should be pointed out that none of these electrodes were designed for fast charging. It remains to be seen if these observations hold true at higher capacity loadings. A decision was made in January (2018) to use the SLC1506T graphite from Superior Graphite for the first pouch cell build deliverable in order to meet the deadline for delivery of these pouch cells to the battery testing labs.

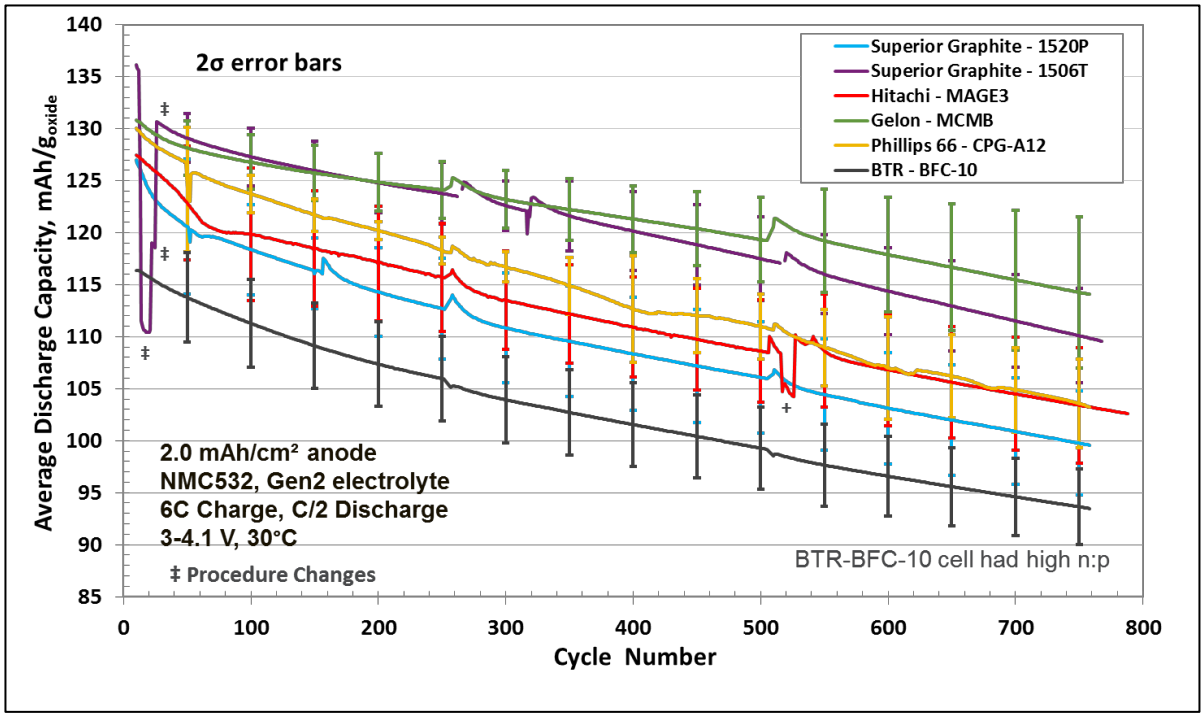

Figure 2. Discharge capacity retention for the graphite materials selected in the coin-cell prescreening study under 6C charge and C/2 discharge between 3 – 4.1V at 30°C (anode capacity of 2 mAh/cm²). +cycler issue

Table 2: Summary of capacity retention for selected graphites and binders in prescreening task. (Discharge Capacity Retention is based on the 10th cycle (6C Chg, C/2 Dchg))

		Average Discharge Capacity Retention (%)		
Graphite Type	Coating Loading (mg/cm²)	At Cycle 750 (%)	# of Cells in Average	2σ [+/-] Standard Deviation at Cycle 750 (%)
Superior Graphite 1520P	6.3	78.5 %	4	3.22
Superior Graphite 1506T	6.4	80.9 %	3	2.12
Hitachi MAGE3 with PVDF	6.4	81.1 %	4	4.34
Hitachi MAGE3 with CMC-SBR	6.3	84.9 %	3	3.06
Gelon MCMB	6.4	87.3 %	5	5.61
CPG A12	6.1	79.7 %	3	4.77
BTR BFC-10	7.2	80.5 %	4	0.22

Earlier work [1] that addressed the effects of capacity loading on rate performance had indicated that cathode capacity loadings above 2 mAh/cm² experienced lithium plating at charge rates as low as 1.5C. This appeared to be in conflict with the observations from the early prescreening results obtained at the beginning of this fiscal year. One difference noted was that the electrodes in reference [1] were made by an outside vendor using an aqueous CMC-SBR binder, while the CAMP Facility electrodes use a NMP-based PVDF binder. To test the binder effect, the CAMP Facility remade the MAG-E3 graphite electrode using a CMC-SBR binder. This electrode was then tested at the 6C charge rate in the same manner as the prescreening graphite materials presented in Figure 2 above. The results of this binder comparison are presented in Figure 3, where one can conclude that there is no significant difference in the capacity fade rate for either binder system. Although, the behavior of the CMC-SBR cells seem to behave in a better predicable manner. Representative cells from each of these cell sets was opened in a glove box and inspected for signs of plating, which is shown in the insets of Figure 3. There were clear signs of lithium plating near the perimeter of the graphite electrode in the cell with PVDF binder, while there was only a light "halo" near the perimeter for the CMC-SBR cell. The influence of binder type should be explored later in cells with higher capacity loadings.

Coin-cell GITT Study

Lithium-ion diffusion coefficients through these different graphite materials is needed to accurately model the electrochemical processes taking place during fast charges. One of the best methods to obtain these coefficients is obtained via the Galvanic Interruption Titration Technique (GITT). The CAMP Facility is providing 15 duplicate coin-cells for each of the graphite materials listed in Table 1 to Argonne's EADL (Ira Bloom). The results of this on-going study are presented in the EADL report. The coin cells were assembled with 15 mm diameter graphite electrodes and 15.6 mm diameter lithium metal counter electrodes using Celgard 2325 separator (25 µm, PP/PE/PP) and Tomiyama 1.2 M LiPF6 in EC:EMC (3:7 wt%) "Gen2" electrolyte. No formation cycles or other cycles were applied to these coin cells so that the EADL could capture the first lithiation electrochemical response. The cells were delivered to EADL and put on test within a few hours of assembly to minimize corrosion of the copper current collector. The list of graphite coin cells produced for this GITT study so far are: MCMB (A-A010), delivered 10/25/17; SLC1506T (A-A015), delivered 12/18/17; SLC1520P (A-A005A), delivered 12/19/17; and MAG-E3 (A-A016), delivered 2/22/18. The BTR-BFC-10 and A12 graphite cells will be produced later if needed.

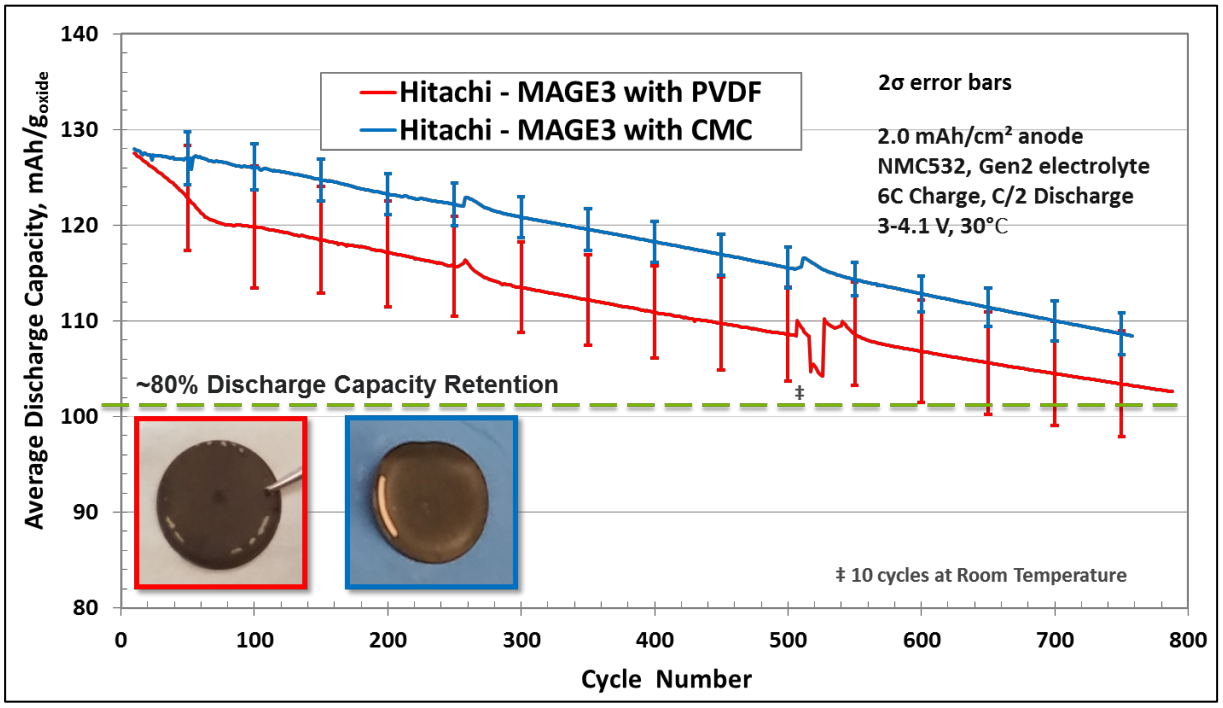

Figure 3. Discharge capacity for the MAG-E3 graphite using CMC-SBR binder versus NMP-based PVDF binder in the coin-cell prescreening study under 6C charge and C/2 discharge between 3 – 4.1V at 30°C (2 mAh/cm²).

Round 1 Pouch Cell Deliverables (Single-sided Single-layer)

Pouch cells were assembled with 14.1 cm² single-sided cathodes (0.145 grams of NMC532 per pouch cell) and 14.9 cm² single-sided graphite anodes (SLC1506T from Superior Graphite) using Celgard 2320 separator (20 µm, PP/PE/PP) and 0.5 mL of Tomiyama 1.2 M $LiPF_6$ in EC:EMC (3:7 wt%) "Gen2" electrolyte. The n:p ratio is between 1.12 to 1.22 for this voltage window (3.0 to 4.1V). After assembly, the pouch cells underwent formation cycles at ~4 psi in the 3.0 to 4.1V window as follows: 1.5V tap charge and hold for 15 minutes, followed by a 12 hour rest, and then 3 cycles at C/10, followed by 3 cycles at C/2. The cells were then brought to a safe state of charge by constant voltage charging to 3.5V for 6 hours, and then degassed, and prepared for shipping/delivery to the battery test labs. A nominal C/3 capacity of 19 mAh was recommend for future tests.

INL requested 30 of these pouch cells for testing. These 30 cells were received at INL the week of 2/13/18. Argonne's EADL requested 16 of these pouch cells for testing in February. These 16 cells were delivered to Argonne on 2/15/18 in 4 test fixtures at ~4 psi. An additional 16 pouch cells were assembled and kept dry (no electrolyte) for Argonne's EADL for future rounds of testing. These additional cells were later filled with electrolyte and electrochemically formed by the CAMP Facility and delivered to EADL on 5/17/18.

In addition, NREL requested 4 of these pouch cells fully formed similar to INL and Argonne's EADL pouch cells for micro-calorimetry studies. They also requested 2 dry pouch cells and several punched pristine anodes and cathodes that are used in the pouch cells. All of these cells and electrodes were shipped to NREL at the end of February. NREL also requested 4 graphite (SLC1506T) half-cell pouch-cells and 4 NMC532 half-cell pouch-cells, which were assembled with no electrolyte (dry) and shipped to NREL the week of 5/28/18.

Round 2 Pouch Cell Deliverables (Single-sided Single-layer)

Several options were available in designing the second pouch cell build. These options included changing the graphite, binder, and electrode capacity loading. Since the results from designing the first cell build indicated that the choice of graphite and binder were not the dominant driving factor in the fast charge performance, it was decided to focus on increasing the electrode capacity loading. As in the 1st pouch cell build, a quick screening was performed to determine an electrode loading that would yield at least a few hundred fast charge cycles. The CAMP Facility searched through their available electrodes with varying electrode loadings to find suitable capacity-matched anode-cathode pairs. Four sets of matched A12 Graphite versus NMC532 were found with nominal loadings of 1.5, 3.0, 4.5, and 5.5 mAh/cm². Coin cells were made with these electrodes and formed at C/10 rate, after which, they were subjected to several 6C charges. It was quite clear from the resulting capacity utilizations that cathode electrode loadings above ~2.5 mAh/cm² were not able to charge at a true 6C rate. (This data was shown at the recent DOE-EERE-VTO Annual Merit Review in June.) Thus, it was decided that the 2nd pouch cell build would use a graphite electrode loading of 3.0 mAh/cm², using the same graphite (SLC1506T from Superior Graphite) and PVDF binder.

Single-sided anode and cathode electrodes were then made with capacity loading of 3.0 and 2.7 mAh/cm², respectively; the n:p ratios were 1.07 to 1.16. Coin cells were assembled with 14 mm diameter cathodes and 15 mm diameter anodes using Celgard 2320 separator (20 μm, PP/PE/PP) and Tomiyama 1.2 M $LiPF_6$ in EC:EMC (3:7 wt%) "Gen2" electrolyte. Eight replicate coin-cells were made and then cycled in the 3.0 to 4.1V window with 3 formation cycles at C/10 (w/ C/20 trickle charge) followed by 3 cycles at C/2 (w/ C/10 trickle charge). After which, 4 of these cells were cycled at a 4C rate and the remaining four were cycled at a 6C rate with trickle charge down to C/5 until a maximum charge time of 15 or 10 minutes, respectively, was reached, with C/2 discharges and 2 minute open circuit rests between charge and discharge steps, for 250 cycles (with 3 cycles at C/2 in between). This profile was repeated until <80% of the capacity measured at the 10th cycle remained.

Figure 4 is a summary of the 2nd Round coin cells compared to the 1st Round coin cells. While at first it appears that the higher capacity loading coin cells (2nd Round) are able to achieve over 700 cycles at a 6C rate, it is apparent that these cells did not perform equally, unlike the 1st Round coin cells which show little cell-to-cell variance in capacity over cycles. Several of the 2nd Round coin cells failed early on and were removed from the figure. In addition, note the large loss of capacity utilization between the cells charged at the 6C rate versus the 4C rate. It will be interesting to see if the 2nd Round pouch cells exhibit similar behavior. The data in Figure 4 was averaged and normalized to the cathode capacity and is shown in Figure 5.

Additional coin cells were built to test the rate capability of the 2nd Round electrodes in full cells. A protocol was written to cycle these cells for 10 cycles at a 1C charge (60 minutes total), then 10 cycles at a 2C charge (30 minutes total), then likewise for 3C, 4C, 5C, and 6C. A C/2 discharge rate was used for each charge cycle. These results are shown in Figure 6 normalized against the weight of NMC532. Data files from this study were provided to NREL for their modeling development.

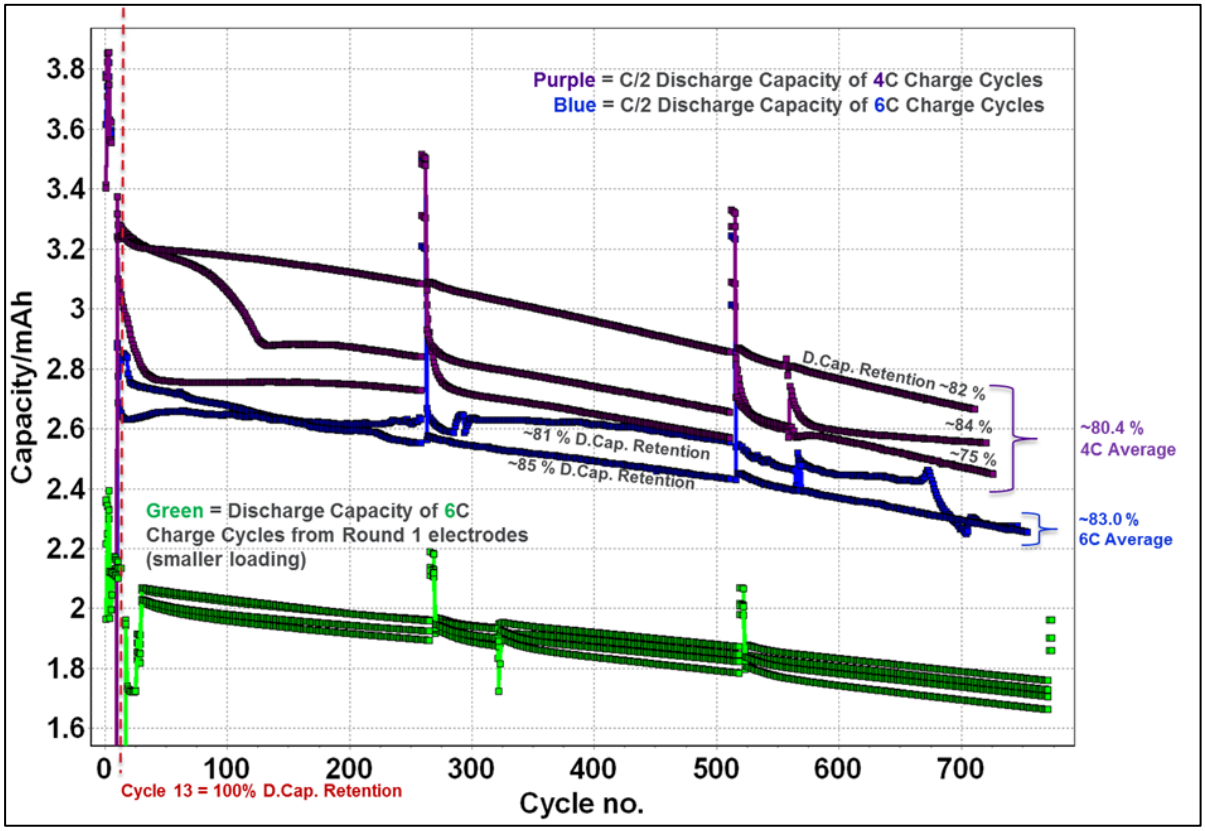

Figure 4. Discharge capacities for the 2nd Round coin cells (Purple and Blue) compared to the 1st Round coin cells (Green) cycled under 6C (and 4C) charge rates (Superior Graphite SLC1506T vs. NMC532).

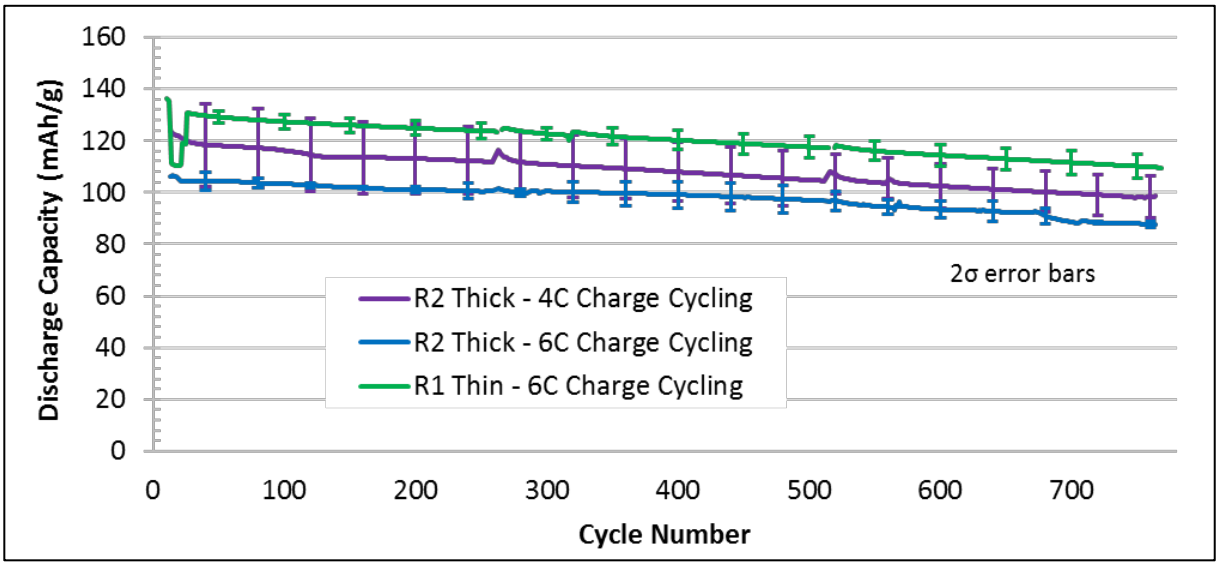

Figure 5. Averaged and normalized capacities (based on NMC532) for the 2nd Round coin cells (Purple and Blue) compared to the 1st Round coin cells (Green) cycled under 6C (and 4C) charge rates (Superior Graphite SLC1506T vs. NMC532).

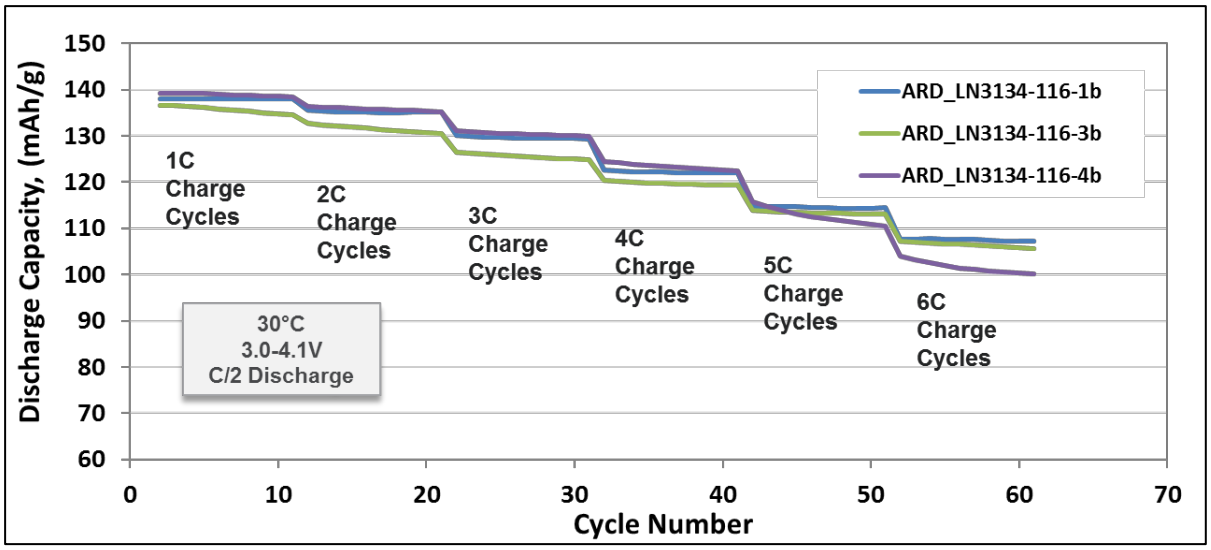

Figure 6. Normalized capacities (based on NMC532) for the 2nd Round coin cells at increasing charge rates (Superior Graphite SLC1506T vs. NMC532).

Pouch cells were assembled with 14.1 cm² single-sided cathodes (0.236 grams of NMC532 per pouch cell) and 14.9 cm² single-sided graphite anodes (SLC1506T from Superior Graphite) using Celgard 2320 separator (20 µm, PP/PE/PP) and 0.615 mL of Tomiyama 1.2 M LiPF6 in EC:EMC (3:7 wt%) "Gen2" electrolyte for an electrolyte-to-pore volume factor of 4.20. The n:p ratio is between 1.07 to 1.16 for this voltage window (3.0 to 4.1V). After assembly, the pouch cells underwent formation cycles at ~4 psi in the 3.0 to 4.1V window as follows: 1.5V tap charge and hold for 15 minutes, followed by a 12 hour rest, and then 3 cycles at C/10, followed by 3 cycles at C/2. The cells were then brought to a safe state of charge by constant voltage charging to 3.5V for 6 hours, and then degassed, and prepared for shipping/delivery to the battery test labs. A nominal C/2 capacity of 32 mAh was recommend for future tests. A plot of the discharge capacities during the formation cycles applied to the 24 pouch cells delivered to INL is shown in Figure 7.

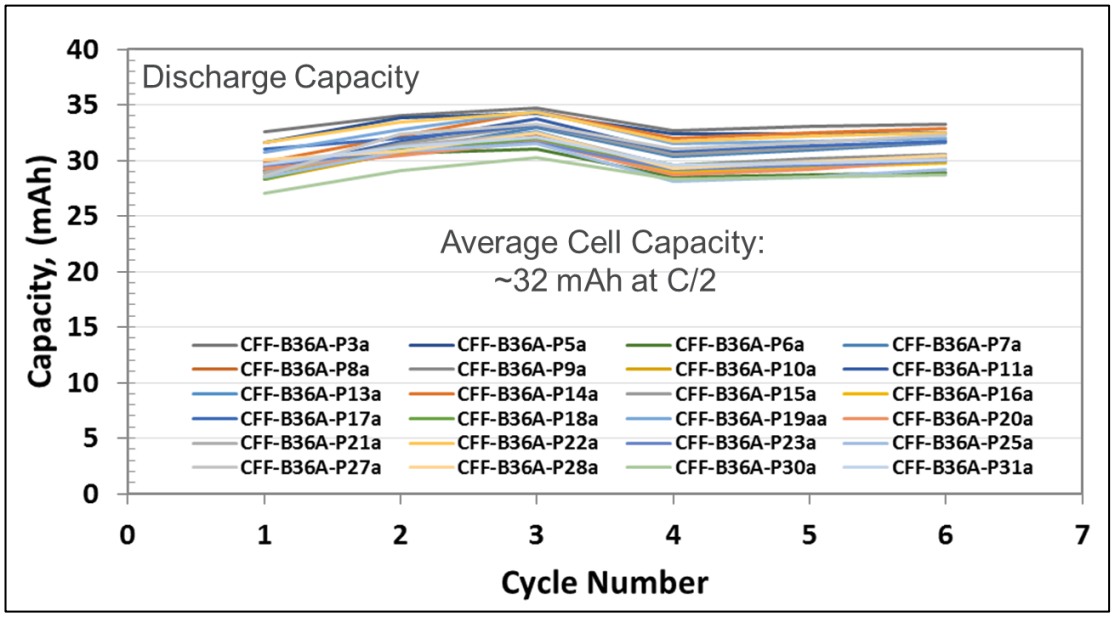

Figure 7. Discharge capacities from formation cycles for 24 single-sided single-layer 2nd Round pouch cells (Superior Graphite SLC1506T vs. NMC532) delivered to INL.

INL requested 24 of the 2nd Round pouch cells for testing. These 24 cells were received at INL the week of 6/18/18. Argonne's EADL requested 16 of the 2nd Round pouch cells, which were assembled, formed, and delivered to EADL on 9/10/18. In addition, NREL requested 4 of the 2nd Round pouch cells fully formed similar to INL's pouch cells for micro-calorimetry studies, which were received at NREL the week of 6/18/18. They also requested 4 dry pouch cells and several punched pristine anodes and cathodes that are used in the pouch cells, and 4 graphite (SLC1506T) half-cell pouch-cells and 4 NMC532 half-cell pouch-cells. These 2nd Round specialty pouch cells were assembled and shipped to NREL on 9/21/18.

Conclusions

Six different graphite negatives were chosen from the CAMP Facility's Electrode Library for fast-charge prescreening and GITT study in coin-cells. Surprisingly similar fade rates were observed at the 6C charge for many of these graphite materials. All of the selected graphites were able to achieve 750 cycles with 80% capacity retention. A decision was made early in the prescreening study to use SLC1506T graphite from Superior Graphite for the first single-sided single-layer pouch cell build using a 2 mAh/cm² graphite loading.

CMC-SBR vs. PVDF binder showed little difference at the 2 mAh/cm² graphite loading.

Over 70 single-sided single-layer pouch cells were fabricated and delivered to lab partners (INL, ANL, and NREL) for fast charge testing with a recommended 19 mAh capacity at the C/3 rate. Half-cell pouch-cells were also designed, fabricated, and delivered to NREL.

Prescreening of anode-cathode pairs with varying electrode capacity loading indicated that loadings over ~2.5 mAh/cm² were not able to charge at a true 6C rate. Thus, the 2nd Round pouch cell build was designed with a graphite loading of 3.0 mAh/cm². 24 of these 2nd Round pouch cells were delivered to INL and 4 were delivered to NREL. 16 of the 2nd Round pouch cells were formed and delivered to Argonne's EADL.

In August of FY18, the XCEL team met with the Awardees from the DOE-EERE-VTO FOA and Lab Call projects related to fast charge. The CAMP Facility has begun supplying these teams with electrodes and pouch cells from the 1st and 2nd Round builds.

Milestones and Deliverables

Status of tasks this quarter and beyond:

B1000 Select candidate materials for first cell builds	9/1/2017 - 11/15/2017	Completed
B1010 Deliver all known characterization information to NREL modeling team for selected graphite candidates	11/1/2017 - 1/31/2018	Completed
B1020 Workshop on lithium plating detection	12/6/2017 -12/6/2017	Completed
B1030 Build and deliver first cell builds to ANL/INL test lab	1/1/2018 - 2/28/2018	Completed
B1040 Second cell builds(single-sided, single layer)	3/15/2018 - 4/27/2018	Delayed 4 wk

References

[1] "Optimizing Areal Capacities through Understanding the Limitations of Lithium-ion Electrodes", Kevin G. Gallagher, Stephen E. Trask, Christoph Bauer, Thomas Woehrle, Simon F. Lux, Matthias Tschech, Bryant J. Polzin, Seungbum Ha, Brandon Long, Qingliu Wu, Wenquan Lu, Dennis W. Dees, and Andrew N. Jansen, *Journal of The Electrochemical Society* 163(2), A138-A149 (2016).

Extreme Fast Charging (National Renewable Energy Laboratory)

Matthew Keyser, Kandler Smith, Shriram Santhanagopalan, Francois Usseglio-Viretta, Weijie Mai, and Andrew Colclasure (NREL)

Background

The NREL team this quarter focused on comparing macro-homogeneous model predictions with experimental test data. In most cases, the model matches experimentally measured data reasonably well. The model is compared to experimental data for cells with the following properties and charging conditions:

- Cell/cathode NMC532 loadings of 1.5 to 5 mAh/cm^2
- Charge rates from C/5 up to 9C
- Anodes composed of Superior 1506T and A12 graphite

For a loading of 1.5 mAh/cm^2 and 1506T graphite at 30°C, cells are capable of withstanding 6C constant current (CC) charging with relatively high capacity of 103 mAh/g-NMC and are free from lithium plating. When the loading is increased to 2.5 mAh/cm^2, the achieved capacity at 6C falls to 51 mAh/g-NMC. Also, ANL and INL data show these cells plate lithium after only 5-10 cycles. The model accurately predicts the falloff in capacity with loading under extreme fast charge (XFC) and shows this falloff is due to electrolyte transport limitations. Requirements for electrolyte transport properties needed to enable XFC of high energy density cells are reported based on model outputs. The report also compares macro-homogenous model predictions with novel in-situ XRD measurements from ANL resolving localized SOC variations across a thick anode. Finally, the tortuosity for a variety of graphite anodes is compared and shown to be linked to particle morphology and alignment within the electrode. In FY19, the validated models will be applied to assess best approaches to achieve 6C charging of energy-dense 3-4 mAh/cm^2 electrodes. These include requirements for next generation electrolytes and electrode architectures.

Results

Figure 1 illustrates 3 main transport limitations that can occur during XFC and their consequences. During charging lithium ions de-intercalate from the NMC positive electrode active particles and transfer into the electrolyte phase. These lithium ions migrate and diffuse from the positive through the separator and into the negative electrode where they intercalate into the active graphite particles. At the high current densities required to support XFC of >10mA/cm^2, large concentration and electrolyte potential gradients develop to drive the necessary flux of lithium ions within the electrolyte. Sustained fast charge can result in electrolyte Li-ion depletion within the negative and/or saturation within the positive electrode. These electrolyte transport limits can also occur at lower charge rates at low temperature and/or for cell designs when electrolyte conductivity is low, electrolyte diffusivity is low, electrode tortuosity is high, porosity is low, and/or electrode thickness is high. Due to limited solid-state diffusivity for graphite and NMC, lithium ions can become saturated at the graphite surfaces and depleted at the NMC surfaces. Saturation of Li ions at

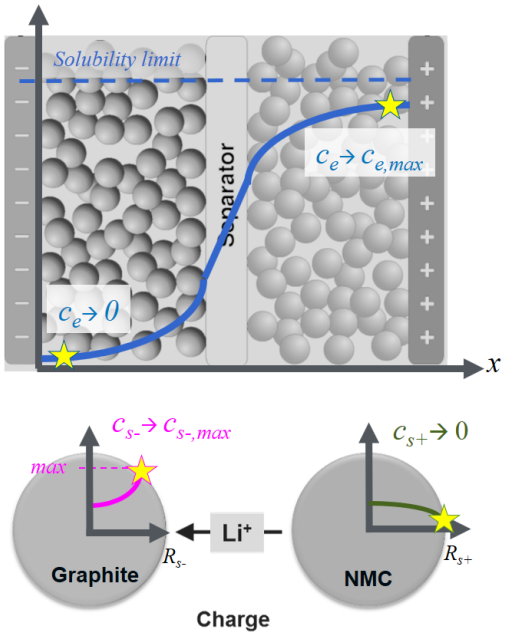

Figure 1. Schematic of the various transport limitations during XFC that can result in poor charge acceptance, heat generation, lithium plating and capacity loss.

the graphite particle surface along with sluggish kinetics can result in lithium plating, causing cell degradation and safety concerns.

The macro-homogeneous model was first compared to high rate charging data for single layer pouch cells with a low loading of 1.5 mAh/cm^2 and results are illustrated in Figure 2. Results are shown for cells with both A12 and Superior 1506T graphite. The anode and cathodes for these two cells are between 40-45 microns with porosities between 33-37%. Both cells have an active area of 14.1 cm^2. The cell with an A12 based anode capacity falls off more when increasing charge rate from 3C to 7C (70% retention) compared to 1506T graphite (80% retention). This is due to the lower tortuosity of the 1506T superior graphite anode that is comprised of more spherical particles. The specific cathode capacity achieved for the 1506T cell at 1,3,5,7, and 9C was 128, 118, 108, 97, and 82 mAh/g-NMC. The model predicts these cells do not suffer from electrolyte depletion.

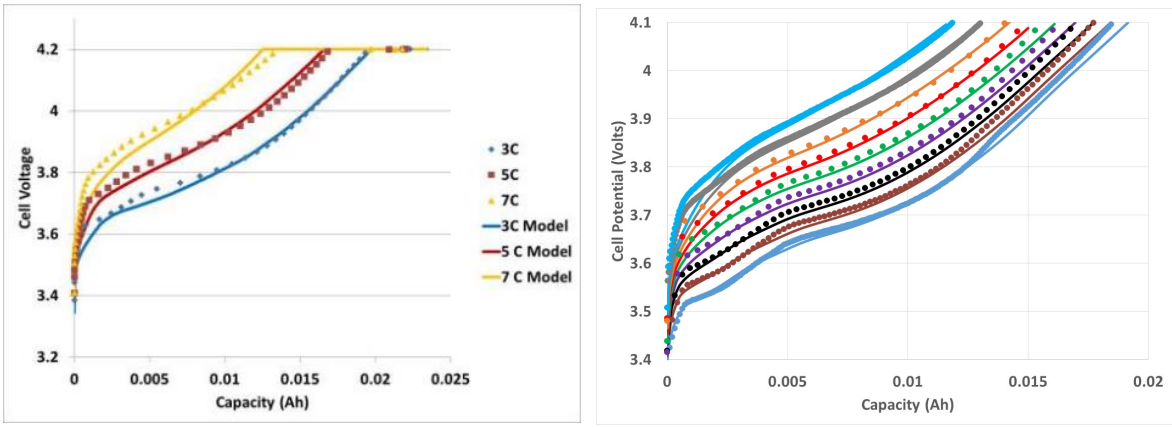

Figure 2. Comparison of high rate charging performance of graphite/NMC 532 cells having a low loading of 1.5 mAh/cm2-NMC. Model results are shown as solid lines and experimental results are dots. The graph on the left is for A12 graphite anode at 3,5, and 7C and the right is for Superior 1506T graphite anode that varies from 1 to 9C.

Next, the model was compared with experimental data for cells with higher loadings and these results are summarized in Figure 3. All cells had an N/P ratio of ~1.1-1.2 and similar porosities of 30-35%. The falloff in capacity with high rate charging for the higher loading cell is well captured by the model. At 6C CC, the specific capacity for A12 cells with a loading of 1.5, 2.8, 4.3, and 5 mAh/cm^2 are 117, 30, 12, and 6 mAh/g-NMC. For the 1506T cell with 2.5 mAh/cm^2 loading, the specific capacity at 1, 3, 5, 7, and 9C was 134, 112, 73, 35, and 17. Thus, the achievable capacity for XFC dramatically reduces with electrode loading. The model predicts this falloff is from electrolyte transport limitations resulting in electrolyte depletion/saturation. This depletion/saturation results in electrodes being preferentially used near the separator interfaces. Electrode material near the current collectors is essentially un-used. While capable of capturing capacity changes, the model significantly under predicts the charge voltage for cells where electrolyte transport is limiting. This could be due to factors such as: uncertainties in electrolyte properties at high concentrations, rate dependent solid diffusivity from cracking/thermal effects, neglecting lithium-graphite phase transitions, and the model using lower tortuosity than predicted by microstructure calculations.

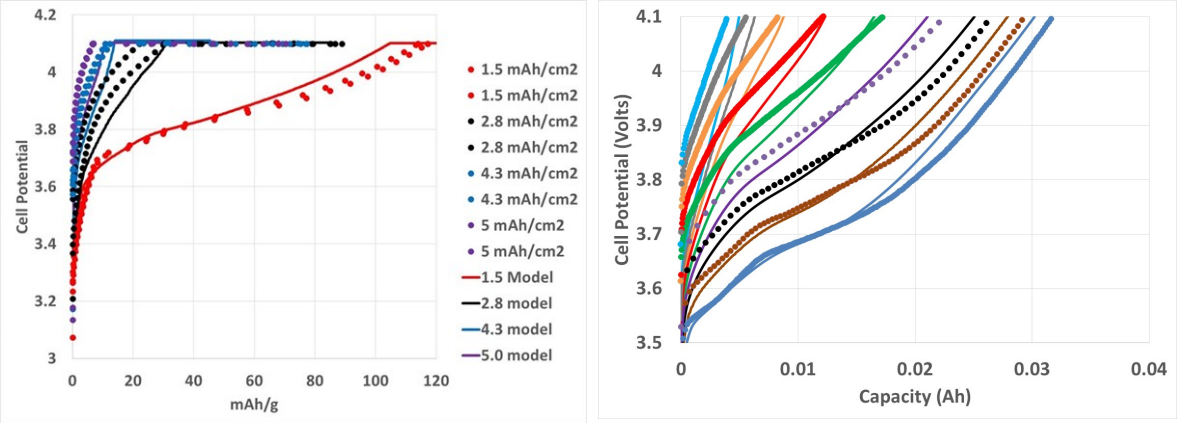

Figure 3. Comparison of high rate charging performance of graphite/NMC 532 cells with higher loadings. Model results are shown as solid lines and experimental results are dots. The graph on the left is for A12 graphite anode at 4 different loadings all charging at 6C (two cells per condition). The right figure is for Superior 1506T graphite anode with a loading of 2.5 mAh/cm^2-NMC and charge rate varying from 1C up to 9C.

NREL's macro-homogeneous model was compared with INL measurements for voltage losses/overpotentials for 1506T cells with 1.5 mAh/cm^2 and 2.5 mAh/cm^2 loading and Figure 4 illustrates the results. INL used rest data after 4.1V cutoff was reached to separate out the voltage losses. The immediate voltage change once current is stopped is an ohmic voltage loss. While the transport loss is measured based on the voltage change after 15 minutes of the cell resting. For the 1.5 mAh/cm^2, the ohmic and transport losses increase with charge rate. However, for the 2.5 mAh/cm^2 loading, the transport losses plateau above 4C indicating major transport limitations.

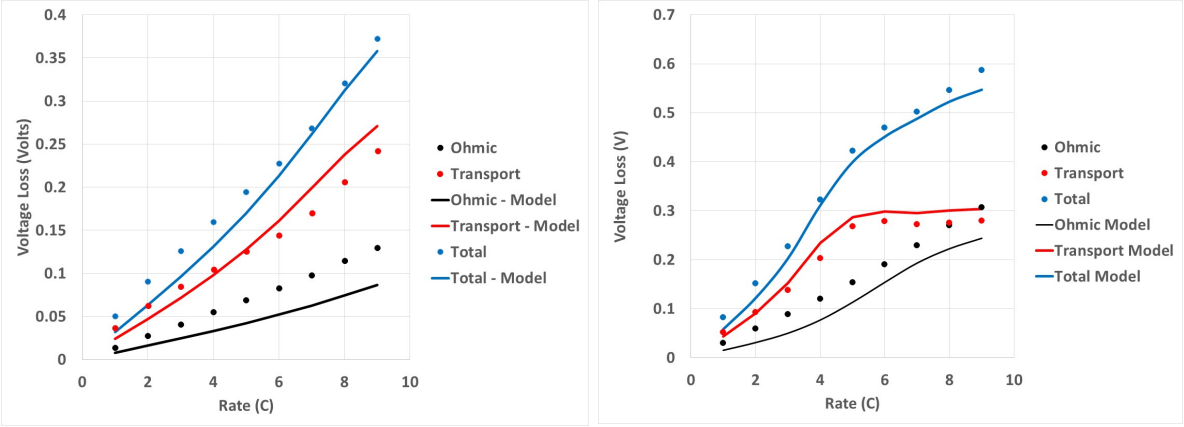

Figure 4. Comparison of transport/ohmic voltage losses as function of charge rate for cells with 1506T anodes at 1.5 mAh/cm^2-NMC (left) and 2.5 mAh/cm^2-NMC (right).. Model results are shown as solid lines and experimental results are dots.

ANL performed in-situ XRD experiments on the Advanced Photon Source (APS) beamline to measure intercalation fraction/SOC within a thick graphite anode during electrochemical cycling. The cell consisted of a 114-micron graphite anode, 25-micron separator, and 111-micron cathode. The cell stage was tilted at different angles to measure the intercalation fraction average within 5 distinct layers during 1C cycling at 30 °C. There was a discrepancy encountered during the discharge portion of the experiment. The intercalation fraction from the 5-layer average did vary linearly with discharge and was higher than expected based on capacity. NREL has had discussions with ANL to try and better understand this discrepancy, but the exact cause is unknown. Thus, to compare with the model, the raw values were divided by a corrective factor such

that the measured average matched the expected value. Layer 0 represents the layer next to the separator and Layer 4 is next to the copper current collector. During charge, lithium is preferentially inserted into the layers closer to the separator. At the end of 1C charging, the intercalation fraction near the separator is 0.9 and only 0.5 at the current collector side due to electrolyte transport limitations. During discharge, lithium is first mainly extracted from the graphite anode near the separator and then eventually lithium is extracted from near the current collector, but only after a significant delay. A 3.0V hold at the end of discharge is needed to remove all the lithium from near the current collector. There is a reasonably good fit between the model predicted intercalation fraction and that measured with in-situ XRD. The model predicts slightly more heterogeneity than measured experimentally. Future experiments are planned to measure the intercalation fraction heterogeneity during higher rate charging, which will require more frequent sampling with better spatial resolution.

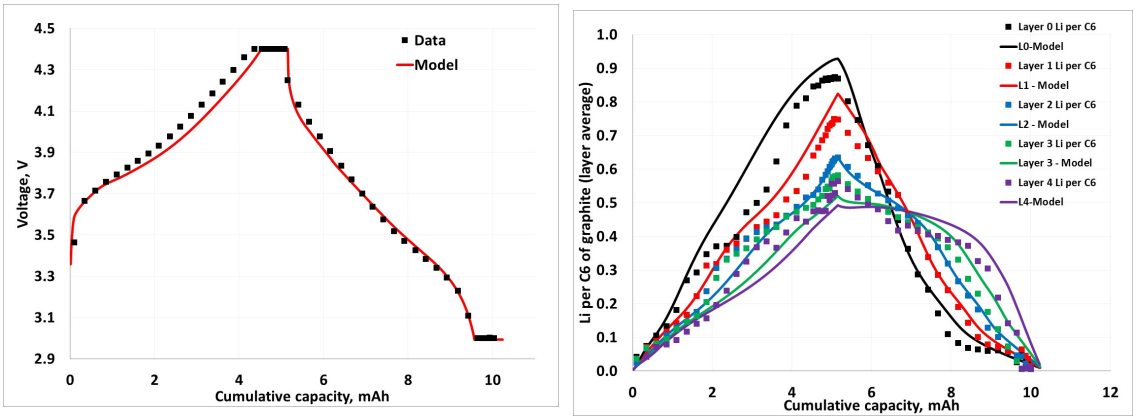

Figure 5. Cell potential and intercalation fraction within A12 graphite anode during 1C in-situ XRD experiments performed by ANL. Experimental results are squares and model predictions are lines. Layer L0 refers to layer closest to separator and L4 is layer next to current collector. Each layer is approximately 20 microns.

After fitting the model to all available data, the macro-homogeneous model is used to predict achieved capacity/SOC and driving potential for lithium plating as a function of loading for 4 and 6C charging (Figure 6). The simulations were run up to a charge cutoff of 4.1 volt. The cathode and anode porosities were set to 33% and 38%, respectively. Using the Superior graphite 1506T results in slightly better rate capability at moderate loadings of up to 10% SOC. The model predicts the round 2 (2.5 mAh/cm^2-NMC) cells at 30°C are right on the verge of having lithium plating. For electric vehicle (EV) applications, a loading of 3.5 mAh/cm^2 or higher is desired. This corresponds to electrodes that are approximately 100 microns thick. The model predicts with the standard Gen2 electrolyte operating at 30°C cells with this loading cannot be effectively charged at 6C.

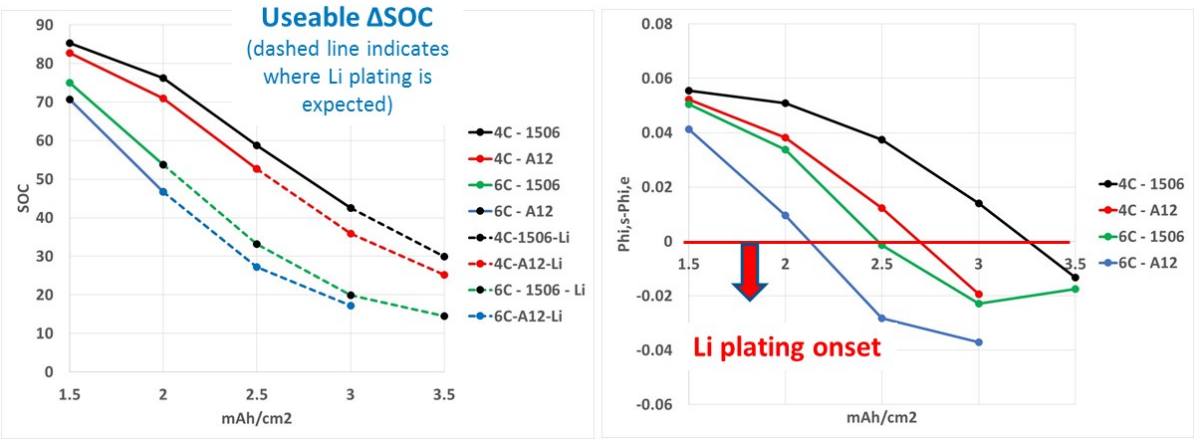

Figure 6. Macro-homogeneous model predictions for useable SOC (left) and driving potential for lithium plating (right) as function of cell/cathode level loading at 4 and 6C. For the capacity plot, the line turns dashed when there is a driving potential for lithium plating.

To enable XFC of energy dense cells with high loadings, it is important to improve electrolyte properties and reduce negative electrode tortuosity. Figures 7 and 8 illustrate how a next generation electrolyte and negative electrode could improve the charge rate capability of thick electrodes. At 30°C and ~1M, the present Generation 2 electrolyte (LiPF6 in 30% wt EC/70 wt% EMC) achieves an electrical conductivity of 10 mS/cm and diffusivity of 1.5e-10 m^2/s. The hypothetical next generation electrolyte has a conductivity of 15 mS/cm and diffusivity of 4.5e-10 m^2/s at 30°C at ~1M and negative electrode has a Bruggeman exponent of 2 (compared to the present negative electrode whose Bruggeman exponent is ~2.5). The model predicts these improvements help prevent lithium plating and electrolyte saturation/depletion for electrodes as thick as 100 µm and at charge rates up to 7C. Other researchers have noted the importance of enhancing electrolyte properties to enable XFC within high energy density cells. Recently, Jeff Dahn and coworkers have published results indicating incorporating ethers as a co-solvent improves electrolyte conductivity with values reported up to 13 mS/cm at 30°C enabling slightly higher rate charging without plating [1-2]. The addition of ethers is also shown to reduce viscosity and thus likely improve diffusivity since the two are inversely related. It should be noted, the present estimate for lithium plating considers very fast lithium intercalation kinetics ($a_s i_o$ = 6 A/cm^3 at 50% intercalation fraction). Further, the model only considers the potential of the electrode phase relative to the electrolyte phase and simple chemistry. More detailed models incorporating SEI chemistry, SEI potential drop, and multiple lithium-graphite phases will be adopted as needed during the XFC project to more accurately predict the onset of lithium plating.

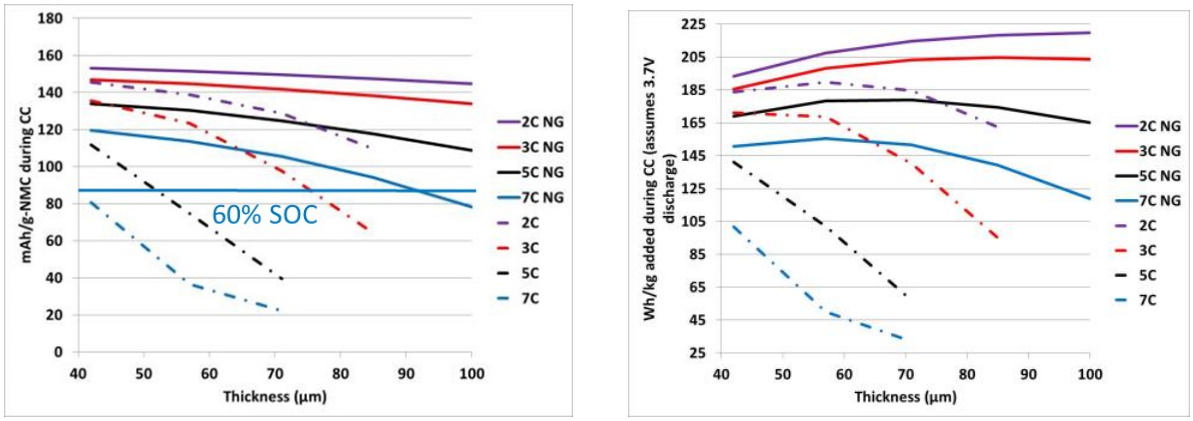

Figure 7. Model predictions for how normalized capacity (left) and energy density (right) achieved during XFC vary with electrode thickness/loading for current electrodes and electrolyte (dot-dash lines) and next generation (NG) electrodes and electrolyte (solid lines).

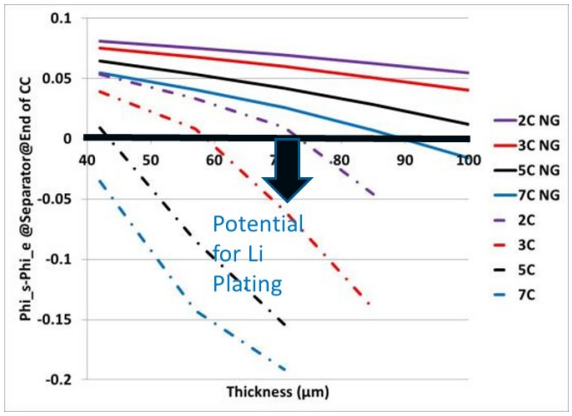

Figure 8. Model predictions for lithium plating during XFC as function of electrode thickness/loading for current electrodes & electrolyte (dot-dash lines) and next generation (NG) electrodes & electrolyte (solid lines).

To quantitatively understand tortuosity of various graphites, NREL also performed detailed microstructure reconstruction/simulations of 6 anode samples from ANL. By combining with electrochemical experimental data, this analysis provides insight into the effect of microstructure properties on the ability of electrodes to handle XFC. First, computed tomography imaging was performed by the University College of London on the anode samples. Then NREL performed segmentation of the images to construct a 3D volume representation. A drawback of the imaging is that it does not distinguish between pores and the carbon binder domain. This phase can have a significant impact on electrode tortuosity. In separate work under the CAEBAT program [3], NREL worked with Purdue University to numerically generate an appropriate carbon/binder phase. Homogenization calculations were performed to determine the effective diffusivity through the 3D microstructure and thus calculate the electrodes' tortuosities. A summary of the measured tortuosity for the different graphite types is illustrated in Figure 9. In general, graphite anodes have higher tortuosity than cathodes with spherical NMC particles. The Superior graphites and MCMB have lower tortuosity than A12

graphite because they have more spherical particles. The 1506T and MCMB have higher 6C charge capacity for 1.5 mAh/cm^2 cells likely from their reduced tortuosity.

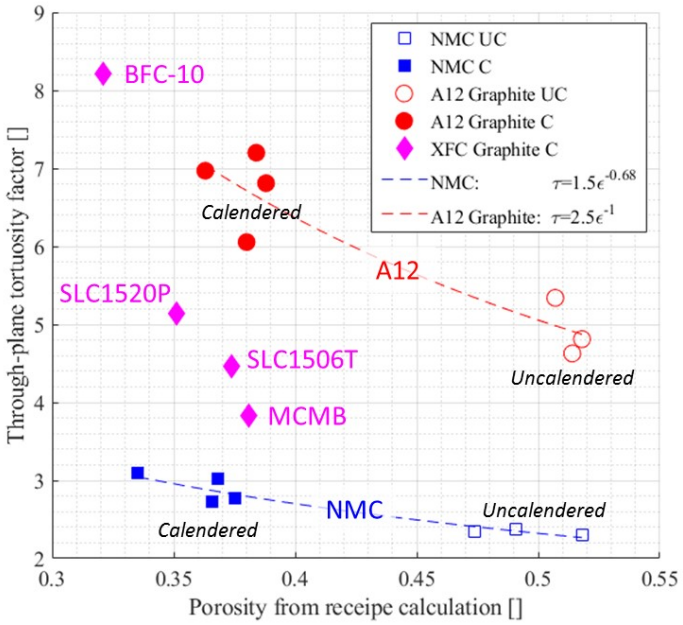

Figure 9. Microstructure predicted tortuosity for several different electrodes.

Conclusions

NREL's macro-homogeneous electrochemical model was compared to extensive experimental data collected by ANL and INL. Across multiple graphite materials and electrode loadings, the model is found to fit data relatively well including cell capacity, measured voltage losses, and intercalation fraction. The model tends to underpredict cell potential during initial charging for thick electrodes and/or high rates with electrolyte transport limitations. Uncertainties that could be responsible include: unknowns in electrolyte properties at high concentrations, thermal/mechanical effects, model using lower anode tortuosity than predicted from microstructure analysis, particle cracking, and simplified electrochemistry. Nonetheless, discrepancy is small. The model further agrees with qualitative observations of lithium plating seen from cell tear downs, though further quantitative analysis is warranted.

The model predicts that, with standard Gen2 electrolyte and 6C charging, electrode loading must be limited to $\leq$ 2.5 mAh/cm^2-NMC. Higher loadings are predicted to have very poor charge capacity acceptance and to plate lithium. Requirements for a hypothetical next generation electrolyte are discussed to enable 6C charging of 100-micron electrodes. Lastly, microstructure analysis/calculations are shown to estimate tortuosity for numerous electrodes. Key to enabling XFC is using electrodes with low tortuosity. For traditional porous electrode architectures, spherical shaped graphite particles provide the lowest tortuosity. Preliminary studies indicate that 6C charge is possible thick 3-4 mAh/cm^2 cells only by combining both improved electrolyte transport properties and lower tortuosity for anode and cathode. Charging at 45 °C also partially alleviates transport limitations. Microstructure studies/analysis in FY19 will help to determine possible electrode architectures that have required tortuosity needed for XFC.

Milestones and Deliverables

NREL FY18Q4 Milestone to DOE, "Comparison of models with test data," September 30th, 2018.

References

[1] ER Logan, EM Tonita, KL Gering, J. Li, X. Ma, LY Beaulieu, and JR Dahn. “A study of the Physical Properties of Li-Ion Battery Electrolytes Containing Esters.” *J. Electrochem. Soc.* 165, A21-A30 (2018).

[2] X Ma, RS Arumugam, L Ma, E Logan, E Tonita, J Xia, R Petibon, S Kohn, and JR Dahn. “A study of Three Ester Co-Solvents in Lithium-Ion Cells.” *J. Electrochem. Soc.* 164, A3556-A3562 (2017).

[3] F.L.E. Usseglio-Viretta, A. Colclasure, A.N. Mistry, K.P. Yao Claver, F. Pouraghajan, D.P. Finegan, T.M.M. Heenan, D. Abraham, P.P. Mukherjee, D. Wheeler, P. Shearing, S.J. Cooper, K. Smith, “Resolving the Discrepancy in Tortuosity Factor Estimation for Li-Ion Battery Electrodes through Micro-Macro Modeling and Experiment,” *J. Electrochem. Soc.* 165, A3403-A3426 (2018)

ANL Modeling: Electrochemical, Atomistic, and Techno-Economic (BatPaC)

Dennis Dees, Hakim Iddir, Juan Garcia, and Shabbir Ahmed (Argonne National Laboratory)

Background

Electrochemical modeling uses continuum based transport equations combined with kinetic and thermodynamic expressions to allow the potential, concentration, and current distributions to be determined throughout the cell. The recent focus of the electrochemical modeling effort is to improve an existing phase change model developed for graphite active materials [1]. The previous model treats graphite active materials as multiple phases, also referred to as stages for graphite, where the well-known Avrami equation was introduced to describe the phase changes as a function of lithium concentration. Further, the model effectively correlated lithium diffusion and phase change during galvanostatic intermittent titration technique (GITT) studies. However, based on limited half-cell (i.e., graphite//lithium metal cell) data with an MCMB graphite electrode, the model tended to underestimate the performance of the graphite at high current rates.

Li-C phases and Li diffusion in graphite are modeled at the atomic scale to characterize the structure of the starting material and its changes during fast charging. Further, bulk defects, surface and edge effects on Li diffusion will be investigated for select conditions.

The Battery Performance and Cost model (BatPaC) was developed for lithium-ion battery packs used in automotive transportation. The model designs the battery for a specified power, energy, and type of vehicle battery. The cost of the designed battery is then calculated by accounting for every step in the lithium-ion battery manufacturing process.

Results

Electrochemical Modeling

Previously this fiscal year, the phase change model was successfully applied to GITT studies on an A12 graphite half-cell that produced a parameter set effectively correlating the experimental results over both charge and discharge. Further, electrochemical modeling on full reference electrode cell studies indicated that the lithium diffusion coefficient through graphite increases with applied current rate. To better understand the functionality between the lithium diffusion coefficient and applied current rate a plot for a wide range of studies (i.e. GITT at C/18, constant charge C/5 to 6C, and HPPC) is shown in Figure 1. A similar functionality was assumed for the lithium diffusion coefficient through graphite used in the electrochemical model as given by the following equation.

$$D_S = Constant\left(\left|\frac{\partial c_S}{\partial y}\right|\right)^{Power}$$

As a first examination of the assumed functionality the model was used to fit previous reference electrode cell studies assuming a power of 1.1. As shown in Figure 2, the electrochemical model could be used to correlate the studies, but not with a single constant. Further studies need to be conducted to better understand this phenomenon.

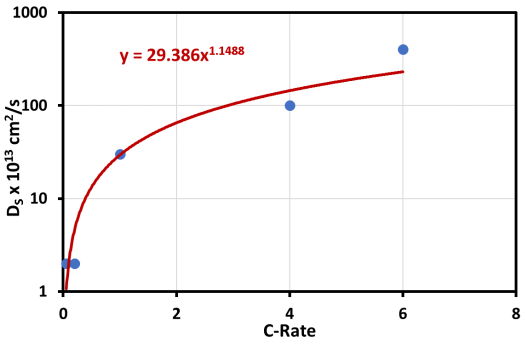

Figure 1. Lithium diffusion coefficient for A12 graphite extracted from electrochemical modeling studies.

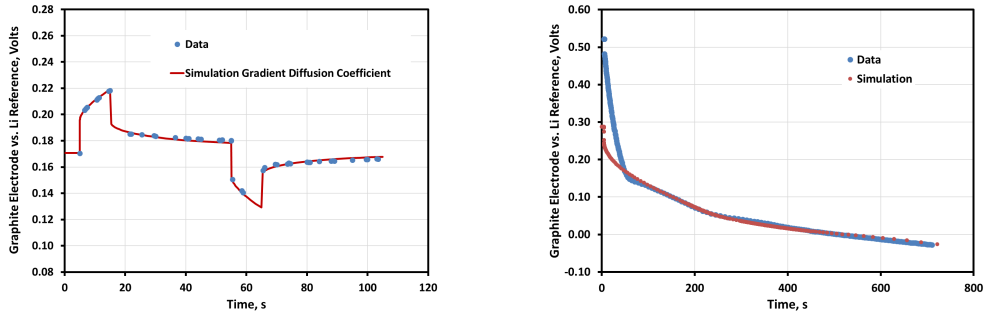

Figure 2. Simulation of graphite electrode data from HPPC (ieft) and 4C Rate Charge (right) on a NMC532 / A12 Graphite reference electrode cell. Constant is $2.5x10^{-14}$ for HPPC and $3.0x10^{-13}$ for 4C charge (i.e. Power equal to 1.1)

Atomistic Level Modeling

Atomistic level analysis of Li-C phases and Li diffusion in graphite will be performed under fast charging conditions. Given the disparity between the electronic and ionic conductivities, an extra electron charge in the system during the initial charging process might be present, particularly near the surface. This un-compensated charge could play a role in the diffusion and staging processes. First, we will study the effect of extra charge in the interlayer spacing in graphite, for several LiC_x phases. Then, we will compute the energy barriers of Li diffusion when extra electrons are present in the system. The effect of the concentrated diffusion of Li atoms for specific configurations will be investigated next. Bulk defects, surface and edge effects on Li diffusion will be investigated for select conditions.

The atomistic simulations will be carried out using a combination of spin-polarized density functional theory calculations, Nudge Elastic bands (NEB) and Kinetic Monte-Carlo using density functional theory (DFT) as implemented in the Vienna Ab Initio Simulation Package (VASP). [2, 3] The exchange-correlation potentials will be treated by the generalized gradient approximation (GGA) parametrized by Perdew, Burke, and Ernzerholf (PBE). [4] The interaction between valence electrons and ion cores will be described by the projected augmented wave (PAW) method. [5] All the ions will be allowed to relax until the total energy differences were no more than 0.003eV. After geometry optimization within the DFT framework, electronic relaxation will be performed using a single point calculation with the hybrid functional HSE06. [6] Analysis of the electronic structure will be carried out using electronic energy and charge density differences, spin density plots and projected density of states (PDOS).

Performance and Cost Modeling

BatPaC is a publicly available spreadsheet tool developed at Argonne for the design of automotive lithium ion batteries and to estimate their cost when manufactured in large volume. [7] It was used in 2017 to estimate the cost of batteries capable of fast charging, defined as being able to recharge 80% of the battery's capacity (from 15% to 95% SOC) in a given time. [8] Based on available data, it was estimated that the battery design was constrained by a maximum allowable current density of 4 mA/cm^2 to prevent lithium deposition in the graphite anode. [9]

These calculations were revisited recently to reflect the changes incorporated in the latest version of BatPaC Version 3.1 (released June, 2018). The changes include the prices of the materials used in the cells. Figure 3 compares the cost estimates for the years 2017 and 2018. The 2018 estimate suggests a non-fast-charging battery cost of \$100/kWh$_{Use}$ based on the following input specifications: [100 kWh$_{Total}$, 85 kWh$_{Use}$, 300 kW, Graphite-NMC622, 168 cells, 315V, production volume of 100K packs per year]. This is \$10/kWh cheaper than the baseline estimate from 2017.

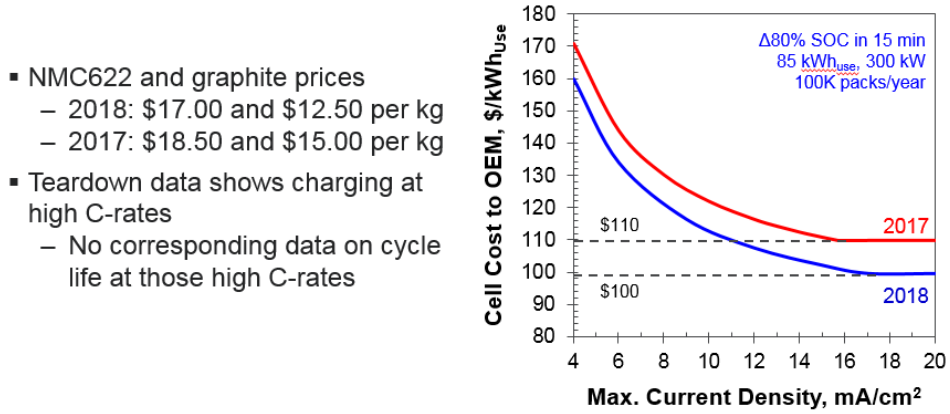

Figure 3. Comparison of cell cost estimates with material prices in 2017 and 2018.

Tests conducted on the cells from a Ford C-MAX battery [10] pack have shown charging up to 80% of the capacity at 5C rate (12 mA/cm^2). However, the data does not include the sustainability of repeated charges at this rate. If we assume that a state-of-the-art anode material in 2018 is capable of sustainably charging at 9 mA/cm^2, then the cost of the cells is estimated at ~\$115/kWh$_{Use}$. The curves also indicate a sharp rise in cell costs at the lower allowable current densities.

Conclusions

Electrochemical modeling indicates the need for a fundamental understanding of increasing diffusion coefficient of lithium through graphite with applied current rate. An atomistic level study has been initiated to address this phenomenon. Updates of BatPaC calculations again emphasize the importance of establishing charge current limitations on pack costs.

Milestones and Deliverables

Improve electrochemical model for graphite to enable fast charge simulation. – Complete

References

[1] K.G. Gallagher, D.W. Dees, A.N. Jansen, D.P. Abraham, and S.-H. Kang, *Journal of The Electrochemical Society*, 159 (12) A2029-A2037 (2012)

[2] Kresse, G.; Furthmüller, J. Efficiency of Ab-Initio Total Energy Calculations for Metals and Semiconductors Using a Plane-Wave Basis Set. *Comput. Mater. Sci.* 1996, *6* (1), 15–50.

[3] Kresse, G.; Hafner, J. Ab Initio Molecular Dynamics for Liquid Metals. *Phys. Rev. B* 1993, *47* (1), 558–561.

[4] Perdew, J. P.; Burke, K.; Ernzerhof, M. Generalized Gradient Approximation Made Simple. *Phys. Rev. Lett.* 1996, *77* (18), 3865–3868.

[5] Blöchl, P. E. Projector Augmented-Wave Method. *Phys. Rev. B* 1994, *50* (24), 17953–17979.

[6] Heyd, J.; Scuseria, G. E.; Ernzerhof, M. Hybrid Functionals Based on a Screened Coulomb Potential. *J. Chem. Phys.* 2003, *118* (18), 8207–8215.

[7] P. Nelson, K. Gallagher, I. Bloom, D. Dees and S. Ahmed, "BatPaC: A Lithium-Ion Battery Performance and Cost Model for Electric-Drive Vehicles," 2018. [Online]. Available: http://www.cse.anl.gov/batpac/.

[8] S. Ahmed, I. Bloom, A. Jansen, T. Tanim, E. Dufek, A. Pesaran, A. Burnham, R. Carlson, F. Dias, K. Hardy, M. Keyser, C. Kreuzer, A. Markel, A. Meintz, C. Michelbacher, M. Mohanpurkar, P. Nelson, D. Robertson, D. Scoffield, M. Shirk, T. Stephens, R. Vijaygopal and J. Zhang, "Enabling fast charging e A battery technology gap assessment," *Journal of Power Sources*, vol. 367, pp. 250-262, 2017.

[9] K. Gallagher, S. Trask, C. Bauer, T. Woehrle, S. Lux, M. Tschech, P. Lamp, B. Polzin, S. Ha, B. Long, Q. Wu, W. Lu, D. Dees and A. Jansen, "Optimizing Areal Capacities through Understanding the Limitations of Lithium-Ion Electrodes," *Journal of The Electrochemical Society*, vol. 163(2), pp. A138-A149, 2016.

[10] Ricardo, "2013 MY Ford C-MAX Energi Battery Cell Teardown Analysis," 2016.

XFC: Performance Characterization and Post-Test Analysis

Contributors (Argonne National Laboratory): David Robertson, LeRoy Flores, Alison Dunlop, Stephen Trask, Bryant Polzin, Andrew Jansen and Ira Bloom

Background

One of the objectives of these projects is to determine how small, pouch cells, which contain selected graphite anodes and oxide cathodes, respond to extreme fast charging. One of the key points here is to detect lithium plating as soon as it occurs using electrochemical methods. Another aspect is to provide materials characterization data, such as X-ray diffraction, Raman spectra, and diffusion coefficient measurements, which can be used to understand the observed performance response and for modeling. Another objective is to determine the physical and chemical changes that extreme fast charging caused. These changes will be characterized by post-test analysis of the fast-charged cells. A suite of materials and surface characterization techniques will be used.

Results

We employed electrochemical methods (dQ/dV calculations) is to detect lithium plating as soon as it occurs. Round 1 cells (thin electrodes) were received from CAMP containing thin NMC532 oxide cathodes and 1506T graphite negative electrodes. They were be charged at 6-C rates (1-C discharge rate) at temperatures of 20, 30, 40 and 50°C to determine the effect of temperature on lithium plating. The testing regime consisted of four 6-C/1-C[1] cycles and one C/20 charge and discharge cycle. This was repeated until a total of 25 cycles were accrued. The $1/Q_0 \times dQ/dV$ vs. cell potential curves (see Figure 1) showed no signature, which may be indicative of lithium plating. Examining the anode material from the 20 and 50°C cells, indeed, showed no signs of plating.

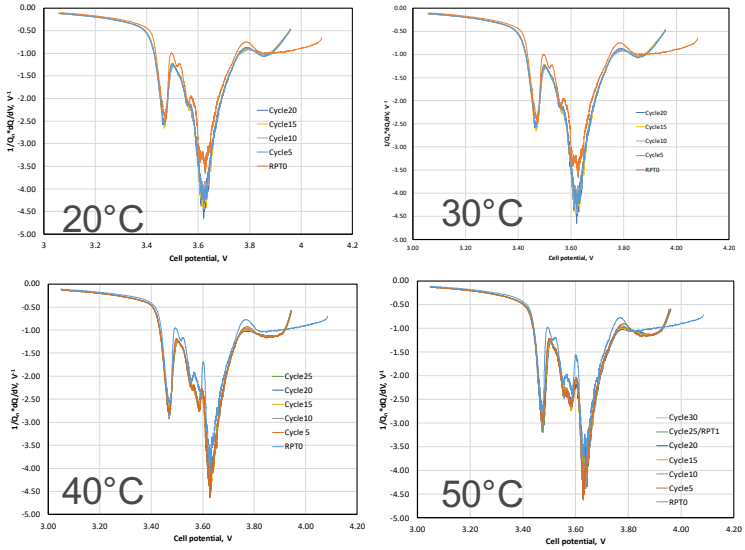

Figure 1. The 1/Q0 × dQ/dV vs. cell potential curves from typical cells in the fast-charge experiment at elevated temperatures.

[1] The charge subcycle was limited to a total of 10 min and consisted of a constant-current/constant-voltage (CC/CV) portions. 1-C was the discharge rate.

After an additional 25 cycles, the test temperatures were lowered to -20, -10, 0 and 10°C to encourage lithium plating and cycling continued. It should be noted that, due to the high resistance of the cells at these temperatures, the upper voltage limit was increased to 4.4-4.6 volt (V) so that the bulk of the charging was performed at the 6-C rate. Again, no signature indicative of lithium plating was seen. After a total of 100 cycles, the anode material was examined for signs of lithium plating. These results are given in Figure 2 and show lithium deposits as grey areas in all of them. The size of the grey seemed to depend on the test temperature and the amount of time spent in the constant-current portion of the charge protocol (see Table 1).

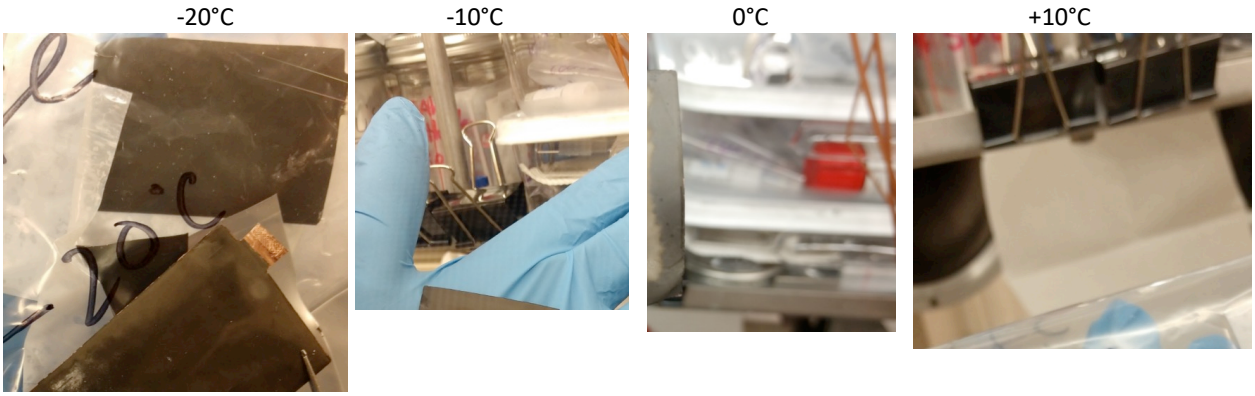

Figure 2. Glove box images of the Round 1 anodes from the fast charge experiment performed at low temperatures.

Table 1. Time spent in the parts of the CC/CV charge cycle.

Temp., °C	Cycle 1		Cycle 50		Cycle 100	
	CC time, s	CV time, s	CC time, s	CV time, s	CC time, s	CV time, s
-20	0	600	0	600	15	584
-10	0	600	5	595	40	560
0	109	491	121	479	289	311
10	282	318	293	307	426	174

Key to color code in table

Charged to 4.6V
Charged to 4.4V

Round 2 cells containing thicker electrodes were tested using the original test temperatures (20, 30, 40 and 50°C). After a total of 5 cycles, the anodes cells from each test temperature were examined for signs of lithium plating. These results are given in Figure 3. Deposits of lithium were apparent as grey areas.

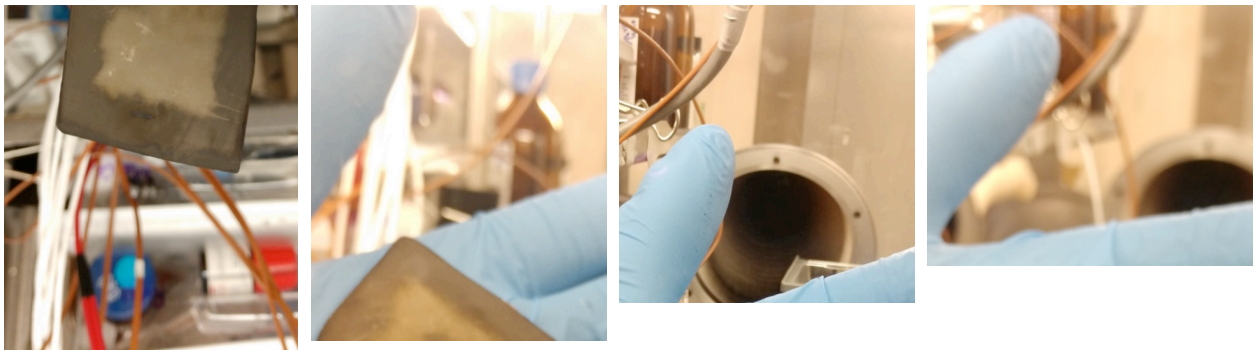

Figure 3. Glove box images of the anodes from Round 2 cells.

Some of these cells later became part of Stanford's efforts.

Conclusions

Round 1 cells. No signature indicative of lithium plating was seen in $1/Q_0 \times dQ/dV$ vs. cell potential curves at low or high temperatures. Post-test examination showed no signs of lithium plating after high temperature testing. When the temperature was lowered to -20 to +10°C, lithium deposits were clearly seen and the area of the deposit seemed to depend on temperature and time spent under high current charging.

Round 2 cells. After 5 CC/CV cycles, cells tested at 20, 30, and 40°C showed clear evidence of lithium plating. The 50°C cell showed none.

Future work

The GITT experiment will repeated in a reference electrode cell. Here, selected graphites will be used as the negative electrode. The experiment will allow the estimation of the diffusion coefficients for both NMC532 positive and the graphite negative electrode.

We gratefully acknowledge support from the U. S. Department of Energy (DOE), Office of Energy Efficiency and Renewable Energy, Vehicle Technologies Office. Argonne National Laboratory is operated for DOE Office of Science by UChicago Argonne, LLC, under contract number DE-AC02-06CH11357.

Extreme Fast Charging R&D: Battery Testing Activities (Idaho National Laboratory)

Eric Dufek (INL), Tanvir Tanim (INL), Daniel Steingart (Princeton)

Background

Extreme fast charging (XFC) of Li-ion batteries can create life and safety issues. Among the issues are shortened battery life due to enhanced loss of lithium inventory and electrolyte degradation and enhanced safety concerns due to potential short creation by Li dendrites. The detection and monitoring of Li plating onset and evolution over aging is a significant challenge. In operando detection schemes to understand the dynamics of Li plating and the role that aging has on Li plating are vital to enable fast charging of specific energy cells.

Discreetly identifying Li plating is difficult without performing a destructive post-test analysis. The objective of the proposed work at INL and Princeton is to overcome these limitations using electrochemical analysis and non-destructive ultrasonic acoustic methods that can be directly applied *in operando* to understand onset and growth of Li plating during XFC. The team is closely coordinating with other efforts at the National Renewable Energy Lab (NREL) and Argonne National Lab (ANL) to understand the key limitations that enhance the probability of Li plating. A key to the efforts is understanding the interplay between materials, electrode structure and use conditions. The ability to understand the interplay will be distinctly aided in this project using the joint electrochemical and ultrasonic tools which ultimately will aid in the scientific understanding required to facilitate the XFC of batteries for electric vehicles.

Electrochemical methods which can be used to identify Li plating include the use of differential capacity (dQ/dV) and quantitative analysis of the cells charge and discharge profiles. These tools give pertinent information associated with both kinetic and thermodynamic processes which occur in batteries, and as such provide direct ability to better understand how variation in materials and electrodes have an impact across the life of a battery. There are limitations on the type of techniques which can be used to compliment electrochemistry in operando using standard cell formats. One method which is showing promise is the use of ultrasonic measurements. Ultrasonic measurements rely on acoustic waves propagating through a structure, such as an electrode, which are modulated by its properties and encode structure/property relationship data. These relationships are directly tied to the material and mechanical changes which occur in a cell during cycling and can be used to characterize change in a non-destructive, real time manner. Coupling ultrasonic and electrochemical measurements will enable a more complete evaluation of the impacts of XFC to be understood. In particular both methods are expected to produce distinct and complimentary signals which signal the deposition of Li on the negative electrode of a battery during aggressive charging conditions. Tracking changes with the coupled ultrasonic and electrochemical methods over life and as batteries age will provide pertinent information related to the distinct conditions which drive Li plating during XFC.

Results

During the fourth quarter of FY18 the primary focus of activities was on the full evaluation of single layer pouch cells received from ANL. The cells were evaluated using 7 different charging protocols (Figure 1) that were specifically chosen to identify different means to impact the transport of Li-ions in the cells. Of the profiles those listed as MS1 had a variable current profile with an initial current as listed, followed by a lower current step, MS2 used a pulsed charge and MS5 used five current steps over the course of the charging. In each case the total time was maintained at 10 min. If the maximum voltage was reached prior to 10 min a constant voltage step was included.

Figure 1 indicates that there was distinct variability over the course of 400 fast charge cycles both across charge profiles and within each profile. Across the profiles the approaches which used 2 current steps appear to have lower variability when compared to other conditions though by a relatively small margin. Thus further analysis of the fade was necessary to more appropriately identify what aging modes were impacting cell

performance. In Figure 1B and 1C, dQ/dV data is shown. From in-depth analysis of the different cells, distinct aging modes were identified. While the cells with the lowest fade displayed primarily loss of lithium inventory (LLI) the higher fade cells also displayed loss of active material (LAM) primarily from the positive electrode side of the cell. This loss of utilization from the positive electrode is most likely attributed by the inability to fully lithiate the NMC during the discharge of the cell due to enhanced LLI. Further analysis (data not shown) highlights that simply looking at capacity and charge-discharge data is insufficient to fully characterize fade. As an example overvoltage data and impedance spectroscopy were jointly used to identify changes which occurred. The overvoltage analysis showed only slight shift in the transport of the cell linked with liquid and solid state diffusion. Likewise, the ohmic impedance had only slight shifts while there was a distinct increase in the charge transfer impedance.

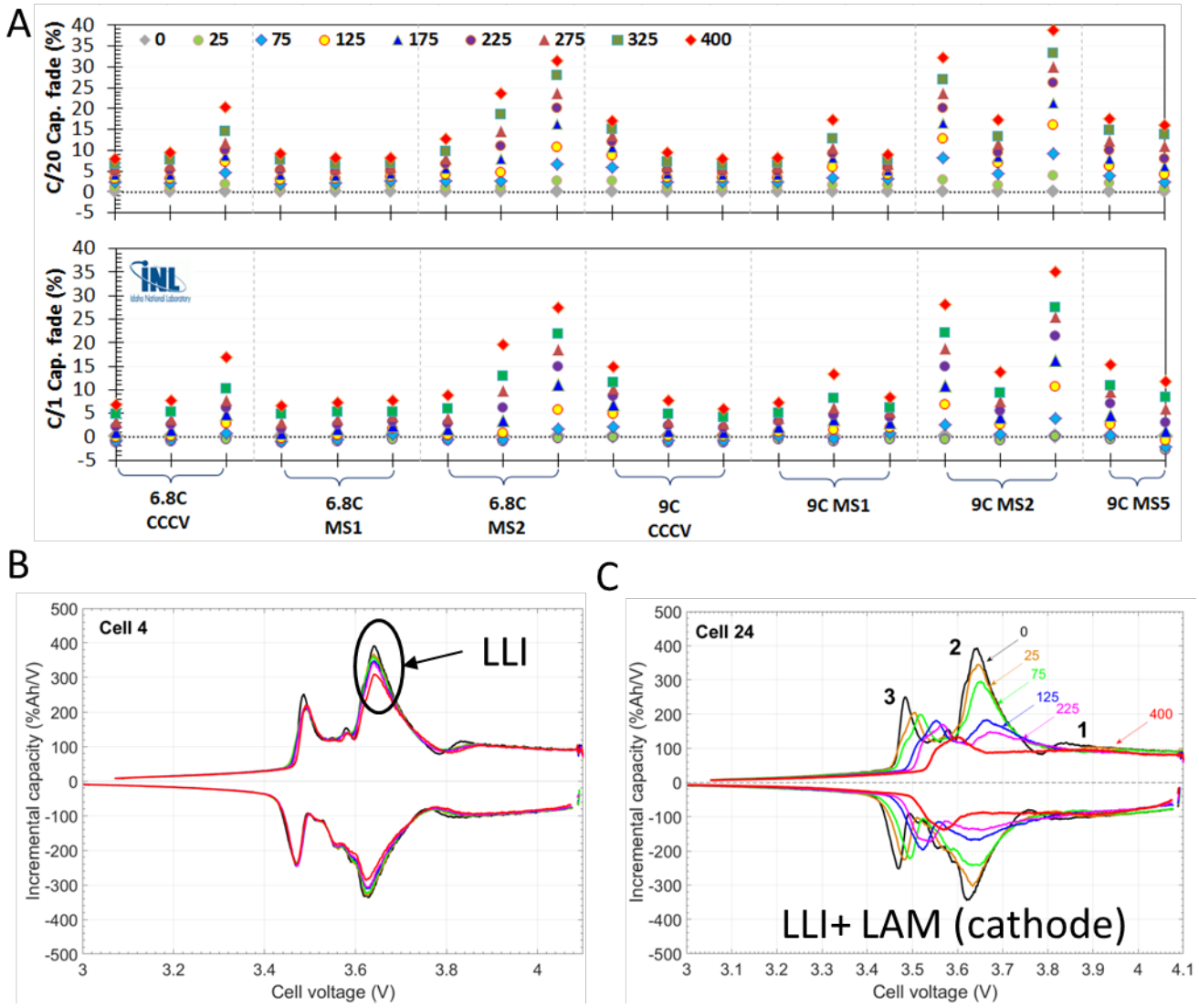

Figure 1: Final results for the fast charging of Round 1 cells (graphite||NMC532). A) Capacity fade at C/1 and C/20 from the reference performance tests B) dQ/dV analysis across testing for one of the lowest fade cells which underwent a 6.8C CCCV profile and C) dQ/dV analysis across testing for the worst performing cell tested using a 9C MS2 profile.

While fade mechanisms were identified using the differential capacity analysis in the fourth quarter, there was not discrete and direct evidence of reversible Li cycling even in cells which were aged in excess of 20%. Indirectly there is evidence of Li plating due to enhanced levels of LLI. The use of other methods to look for

Li plating were also used including ultrasonic evaluation of the single layer cells. In order to increase measurement sensitivity different experimental design options were investigated that by the end of the quarter enabled more direct evaluation of the thin cells. Despite these efforts and in line with electrochemical evaluation there was not distinct, direct detection of Li metal.

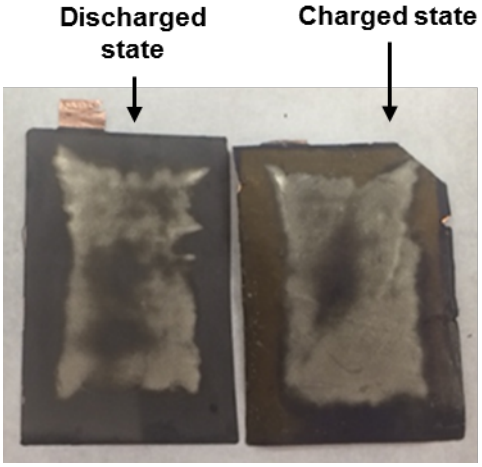

Figure 2: Direct evidence of Li plating for two cells following 10 cycles using 6C CCCV charging. On the left a cell that had been fully discharge and on the right a cell that was disassembled in a charged state.

To address the issue of detecting Li metal a 6C CCCV protocol was used for a second round of cells delivered from ANL which had considerably higher loading at the negative electrode (3 mAh/cm^2). Using this protocol, clear plating of Li was identified following the disassembly of cells. For both a cell that was fully discharged and one that was disassembled while charged there is clear evidence of Li in the central regions of the cell (Figure 2). While qualitative, comparison of the two images in Figure 2 suggests that the bulk of the Li which was plated during the fast charge protocol was irrversibly plated. Understanding this dynamic between reversible and irreversibly plated Li and how it related to the LLI identified in the first round of cycled cells is an on-going effort. The ability to clearly plate Li as seen in Figure 2 is being used to aid in the use of non-destructive methods such as the ultrasonic experiments.

Conclusions

It has been found that variability in performance is prominent for cells undergoing aggressive fast charging. This variability is seen across charging protocols, but is less distinct for cells which use multiple current steps over the course of a 10 minute charge. Across all the samples the dominate fade mode was LLI though cells with higher fade rates also displayed LAM on the positive electrode side of the cell. For the first round of cells direct electrochemical and ultrasonic detection of reversible Li was difficult. In preliminary cycling of cells with higher loading on the negative electrode, clear evidence of irreversible Li was seen. The 6C CCCV procedure is now being used as a baseline for use with other methods to aid in understanding the reversible and irreversible dynamics of Li metal plating during fast charge.

Milestones and Deliverables

Q1 – Identify and initiate acquisition of cells (COTS or CAMP) and establish baseline procedures for initial evaluation (Go/No-go) – *Complete, received 30 Graphite/NMC single layer pouch cells*
Q2 – Assess variation in cells and provide initial understanding on variability and electrode balance. Start initial aging/characterization efforts – *Complete*
Q3 – Perform initial proof-of-concept experiments to identify the impacts of fast charging at the cell level using non-destructive, *in operando* techniques including ultrasonics – *Complete*
Q4- Report summarizing full cell, electrochemical evaluation methods that should be used for analysis of future XFC activities. This includes the ability to identify variability in cells and means to maintain safe operating conditions (SMART). *Complete*

References

None